Supplementary Information for

New insights into the rheology of cohesive granular media

Sandip Mandal, Maxime Nicolas, and Olivier Pouliquen

Olivier Pouliquen
E-mail:olivier.pouliquen@univ-amu.fr

This PDF file includes:

Figs. S1 to S8

www.pnas.org/cgi/doi/10.1073/pnas.1921778117

SI 1: Hertzian-DMT model. We use a second (non-hysteretic) contact force model called the Hertzian-DMT model, where the viscoelastic contact forces are computed using the Hertzian spring-dashpot model and the adhesive force, using a constant adhesion N_c. Fig. S1 shows the variation of the normal elastic force $\boldsymbol{N}_{ij}^{el}$ (green), adhesive force $\boldsymbol{N}_{ij}^{ad}$ (blue), and the total of the two $\boldsymbol{N}_{ij}^{tot}$ (red) normalized by N_c with the normalized normal overlap (δ/δ_{eq}). Using this model, the dynamics of two identical $(m_{eff} = m/2)$ contacting particles in the absence of any external forces is given by the following equation of a non-linear damped oscillator:

$$\frac{m}{2}\frac{d^2\delta}{dt^2} = -\sqrt{\delta}\left(k_n\delta + \frac{m}{2}\gamma_n\frac{d\delta}{dt}\right) + N_c. \quad [1]$$

In the static limit, the left-hand side and the second term on the right-hand side in Eq. 1 are zero, and the balance between the adhesive force and the elastic force (Eq. 1) then yields an equilibrium overlap $\delta_{eq} = (N_c/k_n)^{2/3}$. The quality factor of the oscillator is estimated after linearizing the equation around δ_{eq} as $Q = \sqrt{3}k_n^{2/3}/(\gamma_n m^{1/2} N_c^{1/6})$.

SI 2: Hysteretic Hookean-DMT model. This model, where the particles experience the adhesive force only while detaching, is quite similar to a capillary bridge model but without any finite distance for the detachment. The model is sketched in Fig. S2. The initial loading of a contact continues along the path $ABCDE$ on the green loading branch of slope k_n before reaching a maximum overlap δ_{max}. δ_{max} is saved as a history variable before unloading happens along the path EF on the blue unloading/reloading branch of slope k_n'. Reloading at this moment first occurs along the same branch following FE, until the previous maximum overlap (or load) is reached, and reloading then continues along the path EH on the loading branch; the value of δ_{max} is updated when the next unloading occurs. Unloading otherwise continues along the path EFG before reaching a minimum overlap $\delta_{min} = \delta_{max} - N_c/(k_n' - k_n)$. Unloading further leads to the red adhesive branch, where the grains experience the adhesion along with the repulsion. Unloading continues along the path GI. The value of δ_{min} is also saved before reloading happens again on IJD path on the unloading/reloading branch (there are an infinite number of possible unloading/reloading branches based on the initial unloading point). Reloading then continues on the loading branch for $\delta > \delta_{max}$, with $\delta_{max} = \delta_{min} + N_c/(k_n' - k_n)$. Unloading along the adhesive branch continues again when $\delta < \delta_{min}$. The contact is lost finally, and all the history is erased subsequently. The hysteretic force on the three branches is given as

$$\boldsymbol{N}_{ij}^{hys} = \begin{cases} -k_n\delta, & -k_n'(\delta - \delta_{eq}) \geq -k_n\delta \\ -k_n'(\delta - \delta_{eq}), & -k_n\delta > -k_n'(\delta - \delta_{eq}) > -k_n\delta + N_c \\ -k_n\delta + N_c, & -k_n\delta + N_c \geq -k_n'(\delta - \delta_{eq}), \end{cases} \quad [2]$$

where $\delta_{eq} = (1 - k_n/k_n')\delta_{max}$ on the way of unloading and $\delta_{eq} = (1 - k_n/k_n')\delta_{min} + N_c/k_n'$ on the way of reloading. The model is significantly different from the two non-hysteretic models. Firstly, the minimum pull-off force is load-dependent and is less than N_c if unloading happens below a maximum overlap $\delta_{max} = N_c/(k_n' - k_n)$ corresponding to point C. Secondly, the dissipation can not be quantified through Q only—the ratio k_n'/k_n also plays a role. Therefore, one needs to be cautious about the interpretation of the effects of inter-particle adhesion and material parameters on the flow profiles in an inhomogeneous system like an inclined plane.

SI 3: Coarse-graining. The flow profiles are measured at steady-state in bins of cross-section 20×20 and height 1 and are averaged over five sets with each over a time window of 50. The stress tensor in a bin of volume V is computed from

$$\boldsymbol{\sigma} = \frac{1}{V}\sum_{c=1}^{n_c}\boldsymbol{F}_{ij}\boldsymbol{x}_{ij} + \frac{1}{V}\sum_{p=1}^{n_p} m_p(\boldsymbol{c}_p - \boldsymbol{v})(\boldsymbol{c}_p - \boldsymbol{v}), \quad [3]$$

where n_c and n_p are the total numbers of inter-particle contacts and particles in the bin, and $\boldsymbol{v}$ is the mean velocity of the particles in the bin.

SI 4: Finding a and b for estimating the 'effective' adhesion for the Hookean-JKR model. Fig. S3 shows a contour plot, which depicts the variation of the combined R^2 $(=R^2_{v^s} + R^2_{h_c})$ with a and b, obtained while fitting the power laws to the collapsed data in v^s vs. N_c^{eff} and h_c vs. N_c^{eff} plots. The maximum in R^2 is noted for $a = 1/2$ and $b = 1/4$.

SI 5: Collapses of the velocity, volume fraction, and r.m.s. velocity profiles for the Hookean-JKR model. Fig. S4 shows collapses of the velocity $(v_x(z))$, volume fraction $(\phi(z))$, and r.m.s. velocity $(u(z))$ profiles for nearly the same value of N_c^{eff} in two different cases.

SI 6: A scaling for the dynamic 'effective' adhesion for the Hertzian-DMT model. We follow the same approach for determining the dynamic 'effective' adhesion for the Hertzian-DMT model, as done for the Hookean-JKR model. We obtain $a = 1/3$ and $b = 3/4$ in this case, which yield

$$N_c^{eff} = N_c\left[\left(\frac{N_c}{k_n d^{3/2}}\right)^{1/3}\frac{1}{Q^{3/4}}\right]. \quad [4]$$

We finally obtain two well-defined master curves $v^s(N_c^{eff})$ and $h_c(N_c^{eff})$ (Fig. S5) for all the simulations done for various (N_c, k_n, Q) at 29°.

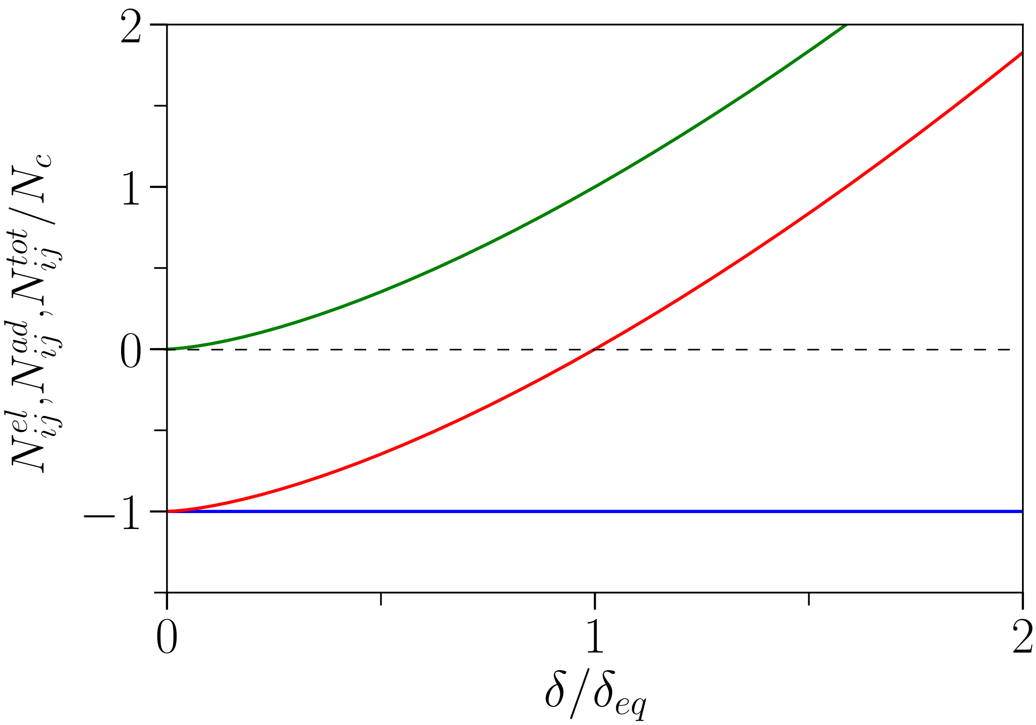

Fig. S1. The non-viscous normal contact forces in the Hertzian-DMT model: elastic $\boldsymbol{N}_{ij}^{el}$ (green), adhesive $\boldsymbol{N}_{ij}^{ad}$ (blue), and the sum of the two $\boldsymbol{N}_{ij}^{tot}$=$\boldsymbol{N}_{ij}^{el}$+$\boldsymbol{N}_{ij}^{ad}$ (red) normalized by N_c as a function of the normalized normal overlap (δ/δ_{eq}). See the text in SI 1 for δ_{eq}.

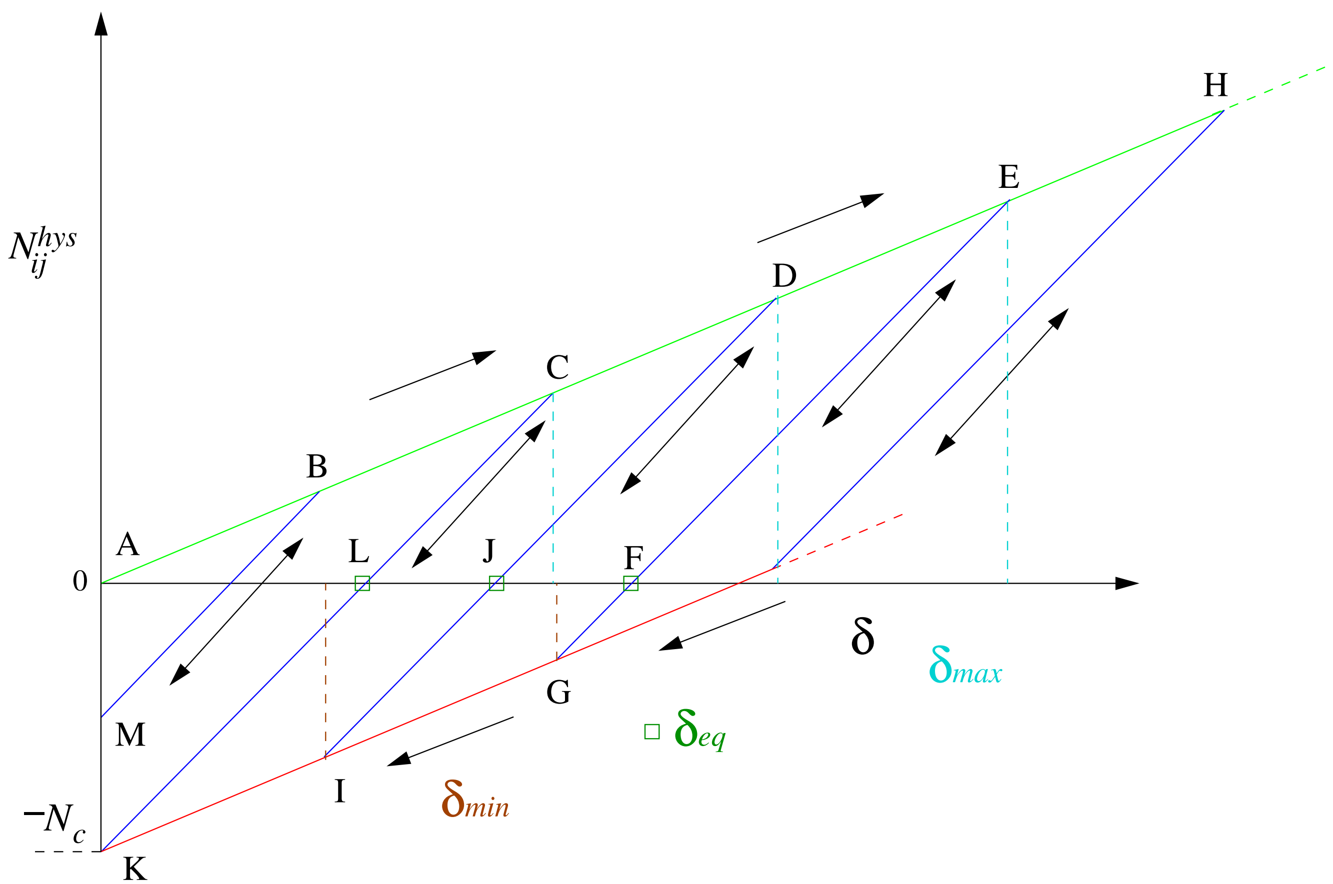

Fig. S2. A sketch of the hysteretic contact model. The arrows show the directions of loading/unloading/reloading. See the text in SI 2.

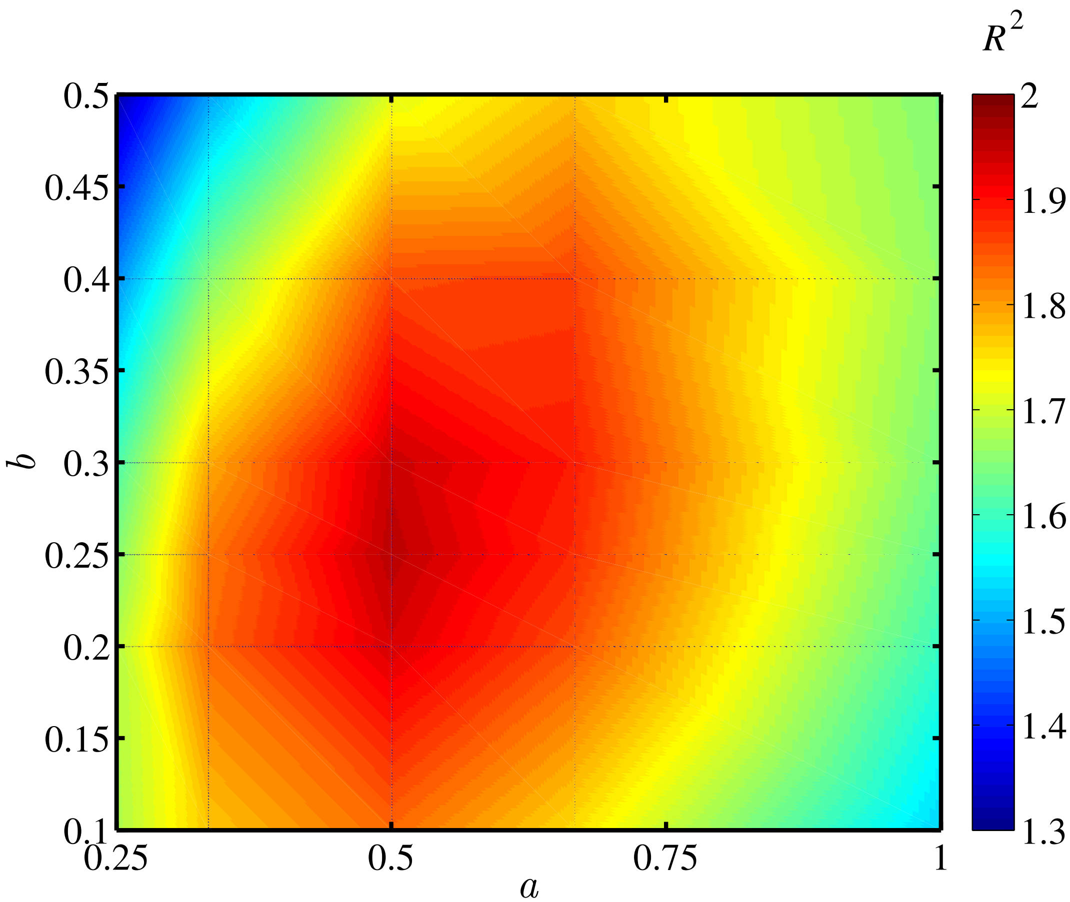

Fig. S3. Variation of the combined R^2 with a and b. See Eq. 2 in the main text.

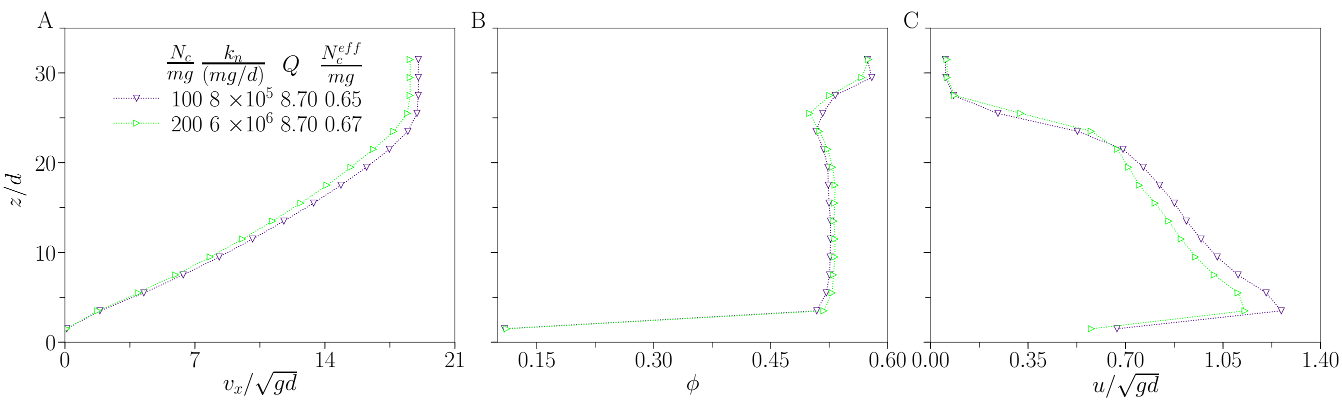

Fig. S4. (A) Velocity ($v_x(z)$), (B) volume fraction ($\phi(z)$), and (C) r.m.s. velocity ($u(z)$) profiles for a similar value of N_c^{eff} but different N_c, k_n, and Q.

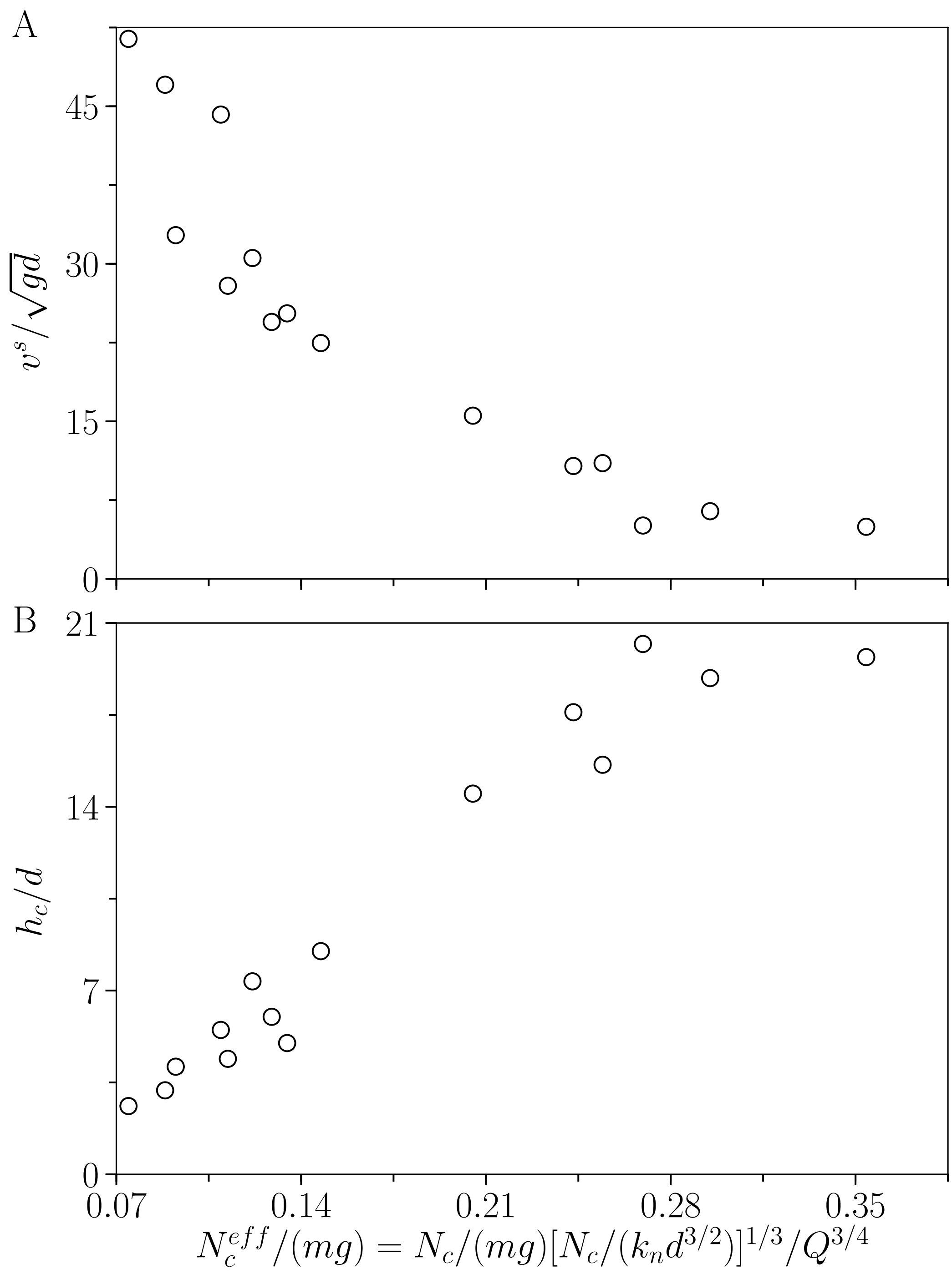

Fig. S5. Evidence of the 'dynamic' effective adhesive force for the Hertzian-DMT model. (A) Variation of the free surface velocity ($v^s/(gd)^{1/2}$) and (B) the thickness of the plug (h_c/d) with the dynamic 'effective' adhesive force N_c^{eff} at $\theta = 29^\circ$ for different $N_c/(mg) \in (25, 100)$, $k_n/(mg/d^{3/2}) \in (10^6, 10^7)$, and $Q \in (9.5, 22.0)$.

SI 7: Evidence of the sensitivity of the bulk cohesion to the material parameters for the hysteretic Hookean-DMT model. The simulations are carried out at a fixed inclination angle $\theta = 22^\circ$ using the hysteretic Hookean-DMT model. The simulation methodology is the same as in the main text, except that the flow is restricted in the xz plane (2D simulations), just for the sake of reducing the computational cost. Fig. S6 shows the effect of the inter-particle adhesion N_c and stiffness k_n on the steady velocity profile. The same behavior of the velocity profile is noticed with increasing N_c and k_n as using the non-hysteretic models. The effect of the dissipation through the quality factor Q on the velocity profile is not so obvious, as mentioned above, hence, is not shown.

SI 8: The fitting of the rheological data using the empirical function proposed by Berger *et al.* (Ref. 27). Berger *et al.* showed that the effective friction μ comprises two parts: (i) a purely frictional part, which is a function of the inertial number I and (ii) a purely cohesive part, which is a function of both I and the cohesion number C. They proposed an empirical function to describe their observations. The function in our case reads as

$$\mu(C^{eff}, I) = \mu(0, I) + \frac{1.31C^{eff}}{1 - \beta \ln\left(1 - I/(1 + \alpha C^{eff})^{1/2}\right)}, \qquad [5]$$

where $\mu(0, I) = \mu_s + (\mu_m - \mu_s)/(1 + I_0/I)$ with μ_s, μ_m, and I_0 be the fitting parameters, and β and α are also the fitting parameters. Fig. S7 shows the $\mu(I)$ data (symbols) for different values of C^{eff} (the data for $C^{eff} > 0.09$ have a few points, hence, are not considered) along with the fits (solid lines) of Eq. 5, taking $\mu_s = 0.37$, $\mu_m = 0.76$, $I_0 = 0.34$, $\beta = 4.0$, and $\alpha = 0.1$. Note that $\mu_s = 0.36$, $\mu_m = 0.75$, and $I_0 = 0.37$ for the cohesionless case ($C^{eff} = 0$) are slightly different. The equation captures the variation of μ with I and C^{eff} well for high I. However, it fails to capture the invariant behavior of $\mu(I)$ at low I for high C^{eff}.

SI 9: Binary collision between cohesive grains. We consider a collision between two cohesive grains with a relative impact velocity v_{init}. The time evolution of the interpenetration δ for the Hookean-JKR model is given by the following dimensionless equation:

$$\frac{d^2\tilde{\delta}}{d\tilde{t}^2} = -\left(2\tilde{\delta} + \frac{1}{Q}\frac{d\tilde{\delta}}{d\tilde{t}}\right) + 2\sqrt{\tilde{\delta}}, \qquad [6]$$

where $\tilde{\delta} = \delta/\delta_{eq}$ and $\tilde{t} = t\sqrt{k_n/m}$. The above equation for the Hertzian-DMT model reads as

$$\frac{d^2\tilde{\delta}}{d\tilde{t}^2} = -\tilde{\delta}^{1/2}\left(2\tilde{\delta} + \frac{\sqrt{3}}{Q}\frac{d\tilde{\delta}}{d\tilde{t}}\right) + 2, \qquad [7]$$

where $\tilde{\delta} = \delta/\delta_{eq}$ and $\tilde{t} = t\sqrt{k_n/m}\,(N_c/k_n)^{1/6}$. In both cases, one can show from the above equations that the two grains will be glued together ($\tilde{\delta} > 0$) after impact if the relative impact velocity $\tilde{v}_{init}$ is less than a critical value $\tilde{v}_c$, i.e., $\tilde{v}_{init} < \tilde{v}_c$. In the above two equations, Q is the only parameter, hence, $\tilde{v}_c$ is a function of Q only. In the dimensional form, $v_c = \delta_{eq}\sqrt{k_n/m}F_1(Q)$ for the Hookean-JKR model and $v_c = \delta_{eq}\sqrt{k_n/m}\,(N_c/k_n)^{1/6}\,F_2(Q)$ for the Hertzian-DMT model. The critical relative kinetic energy is $E_c = 1/2mv_c^2$. E_c for both the models can be given as

$$E_c = N_c\delta_{eq}G(Q), \qquad [8]$$

where $G(Q)$ is a decreasing function of the quality factor, which depends on the chosen model.

SI 10: Planar shear flow simulations. We study the plane shear flow of cohesive grains using a normal stress imposed shear cell in the absence of gravity. The geometry comprises two rough walls composed of randomly glued grains. The top wall is moved with a constant velocity U in the x-direction under an imposed vertical stress $\boldsymbol{\sigma}_{zz}^{ext}$, while the bottom one is kept static. The inter-particle contact forces are computed using the Hookean-JKR model. The top wall movement is governed by the equations of motion based on the balance between the cumulative vertical force $\boldsymbol{F}_{zz}$, exerted on the wall by the flowing particles and the external force $\boldsymbol{F}_{zz}^{ext} = \boldsymbol{\sigma}_{zz}^{ext}A$, where $A = 20d \times 20d$ is the cross-sectional area of the wall. The shear rate is varied by changing U. The results are obtained at steady state (reached when $\boldsymbol{F}_{zz}^{ext} = \boldsymbol{F}_{zz}$) over a strain window of 4 and are made dimensionless using d as the length scale, $(m/\sigma_{zz}^{ext}d)^{1/2}$ as the time scale, and $\sigma_{zz}^{ext}d^2$ as the force scale. Two different sets of parameters (N_c, k_n, Q) yielding the same C^{eff} are considered. The computations of N_c^{eff}, C^{eff}, I, μ, and ϕ are the same as described in the main text. Fig. S8 shows the variation of μ and ϕ with I for the two sets; each cluster of points corresponds to a different shear rate at a given U. The combined data for the same C^{eff} from the inclined plane is also included for comparison. The data of μ and ϕ for the two sets collapse well on each other over the considered range of inertial number. Moreover, the data obtained in the shear cell match reasonably well (the difference is less than 5%) with that in the inclined plane. These results again validate our model.

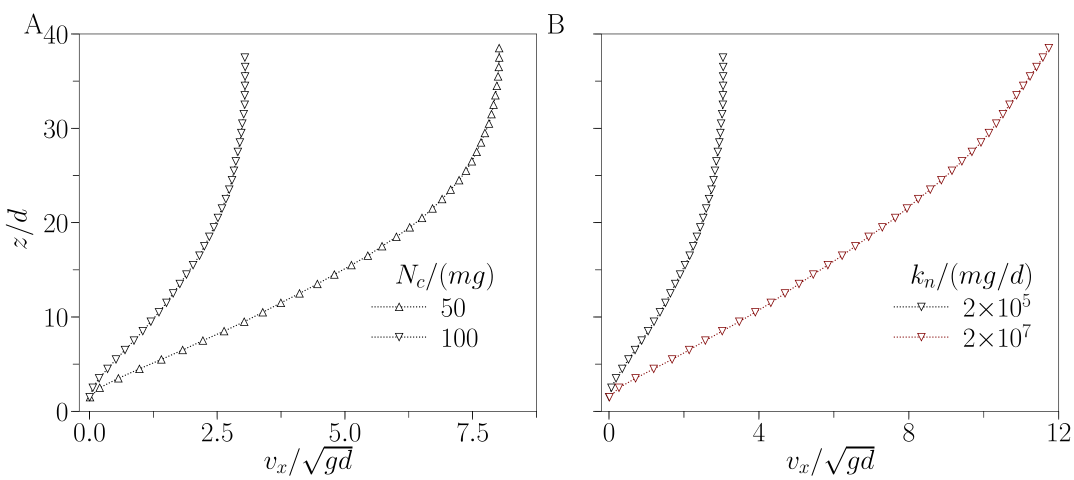

Fig. S6. Effects of particle properties on the flow for the hysteretic Hookean-DMT model. Steady velocity profiles ($v_x(z)$) at $\theta = 22^\circ$ for various (A) inter-particle adhesion (N_c) keeping $k_n/(mg/d) = 2 \times 10^5$ and $Q = 0.94$ fixed and (B) particle stiffness (k_n) keeping $N_c/(mg) = 100$ and $Q = 0.94$ fixed. $k_n' = 2k_n$ in both cases.

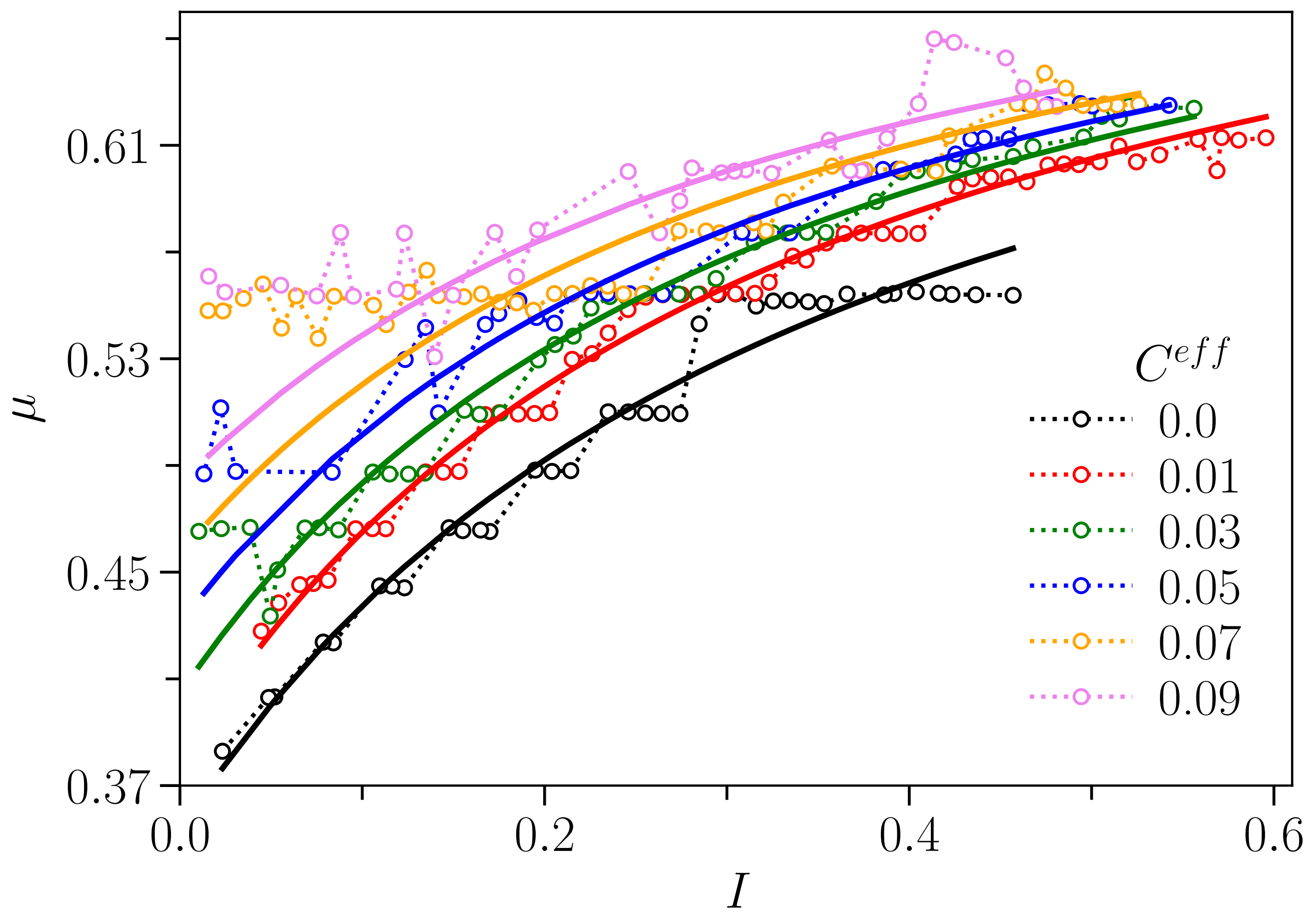

Fig. S7. Fitting of $\mu(I, C^{eff})$ using the empirical function (Eq. 5). The symbols are the data, and the solid lines, the fits.

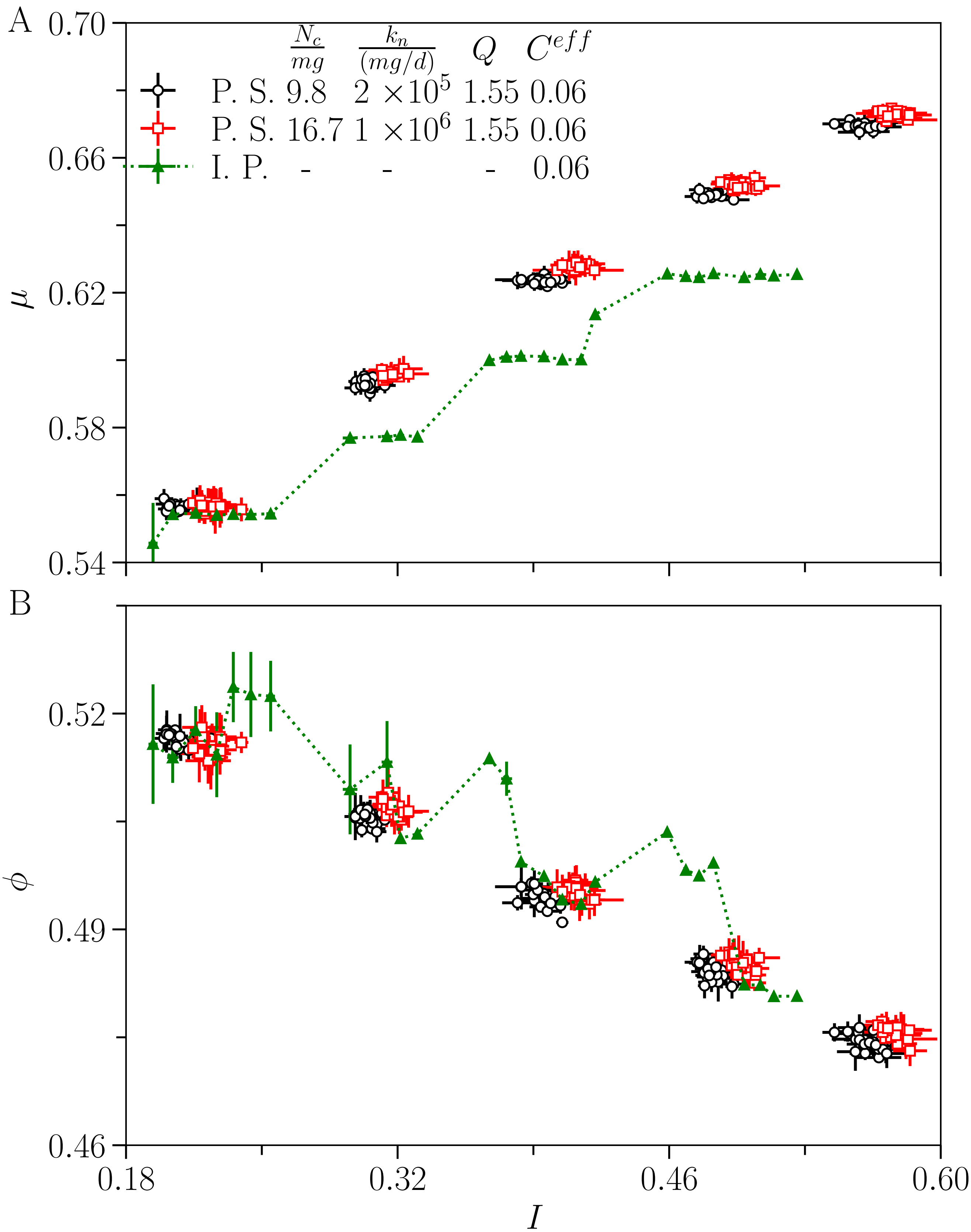

Fig. S8. Comparison of the rheological data of plane shear and inclined plane flows. Variation of (A) the effective friction (μ) and (B) the volume fraction (ϕ) with the inertial number (I) for the same value of 'effective' cohesion number ($C^{eff} = 0.06$), resulting from different (N_c, k_n, Q).